How to Measure the Controllability of an Infectious Disease?

Kris V. Parag⊙*

*MRC Centre for Global Infectious Disease Analysis, Imperial College London, London, United Kingdom
and NIHR HPRU in Behavioural Science and Evaluation, University of Bristol, Bristol, United Kingdom*

Quantifying how difficult it is to control an emerging infectious disease is crucial to public health decision-making, providing valuable evidence on if targeted interventions, e.g., quarantine and isolation, can contain spread or when population wide controls, e.g., lockdowns, are warranted. The disease reproduction number R or growth rate r are universally assumed to measure controllability because $R = 1$ and $r = 0$ define when infections stop growing and hence the state of critical stability. Outbreaks with larger R or r are therefore interpreted as less controllable and requiring more stringent interventions. We prove this common interpretation is impractical and incomplete. We identify a positive feedback loop among infections intrinsically underlying disease transmission and evaluate controllability from how interventions disrupt this loop. The epidemic gain and delay margins, which, respectively, define how much we can scale infections (this scaling is known as gain) or delay interventions on this loop before stability is lost, provide rigorous measures of controllability. Outbreaks with smaller margins necessitate more control effort. Using these margins, we quantify how presymptomatic spread, surveillance limitations, variant dynamics, and superspreading shape controllability and demonstrate that R and r measure controllability only when interventions do not alter timings between the infections and are implemented without delay. Our margins are easily computed, interpreted, and reflect complex relationships among interventions, their implementation, and epidemiological dynamics.

Subject Areas: Biological Physics, Complex Systems,
Interdisciplinary Physics

I. INTRODUCTION

Understanding and quantifying the effort required to control or contain outbreaks is a principal goal of infectious disease epidemiology [1]. During emergent stages of a potential epidemic, when populations are immunologically naive, assessments of disease controllability provide critical evidence on whether targeted interventions, for example, contact tracing, isolation, and quarantines, are sufficient to curb spread [2] or whether nonselective control actions, such as population-level lockdowns and closures, are necessary [3]. These assessments typically rely on mathematical models [4] that combine disease surveillance data (e.g., infection times and cases) with intervention mechanisms (e.g., how isolation interrupts transmission chains) to estimate controllability (in some sense) and have informed the public

*Contact author: k.parag@imperial.ac.uk

health responses for influenza, measles, SARS, Ebola virus disease, and COVID-19, among others [2,3,5–7].

Despite these applications, a systematic and rigorous definition of controllability is lacking [8–10]. While key factors influencing the difficulty of controlling epidemics such as transmissibility, superspreading levels, the efficiency of contact tracing, and the proportion of presymptomatic infections are known [1,8,11], studies generally compute the reproduction number R, or (less commonly) the epidemic growth rate r, under proposed interventions to measure controllability [12]. For example, the impact of contact tracing and presymptomatic spread on controllability are assessed by how they effectively change R [1,13,14]. Here we use R and r to generally indicate the (constant) controlled reproduction number and growth rate subject to some control action or intervention. If no controls are applied, these become the popular basic reproduction number and intrinsic growth rate. The relationship between R and r depends on the pathogen generation time distribution [15] w, which describes the times between infections.

As $R = 1$ or $r = 0$ defines critical epidemic stability, i.e., the state where infections will neither grow nor wane [4], it seems reasonable to base controllability on the distance of $R - 1$ or $r - 0$. Stable epidemics have waning infections ($R < 1, r < 0$) and unstable ones ($R > 1, r > 0$) feature

exponential growth. We therefore expect that larger R or r values signify reduced controllability, justifying stronger interventions, while smaller values imply augmented robustness to transmissibility changes or intervention relaxations. The common interpretation of these distances is that we must scale infections by $1/R$ within timeframes proportional to $1/r$ to reach critical stability [12]. This interpretation further underlies related measures of intervention efficacy such as the herd immunity threshold (i.e., the proportion of the susceptible population that must be vaccinated or acquire immunity) [4,12] and the proportion of infections that must be targeted by contact tracing [2] (both relate to $1-1/R$), as well as the speed at which isolation or digital tracing [9,13,16] must be applied to suppress infections (both relate to doubling time $\log(2)/r$).

In this study, we prove that the above interpretations are only valid under impractical and quite restrictive assumptions. We start by recognizing that, intrinsically, an epidemic represents a positive feedback loop between past and upcoming infections [see Fig. 1(a)]. Interventions are then

(a) Control actions disrupt the positive feedback loop driving infectious disease transmission
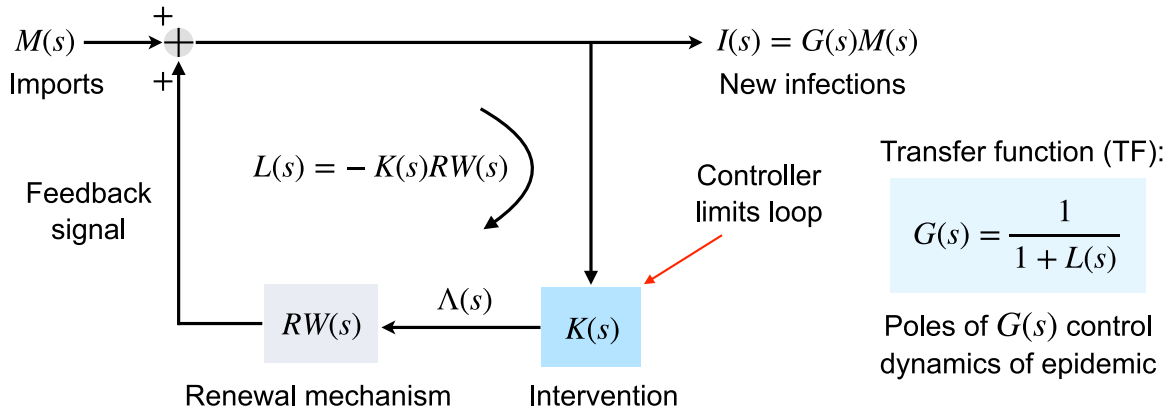
(b) Epidemic controllability defined by margins (M_G, M_D) of $L(s)$ from critical stability point
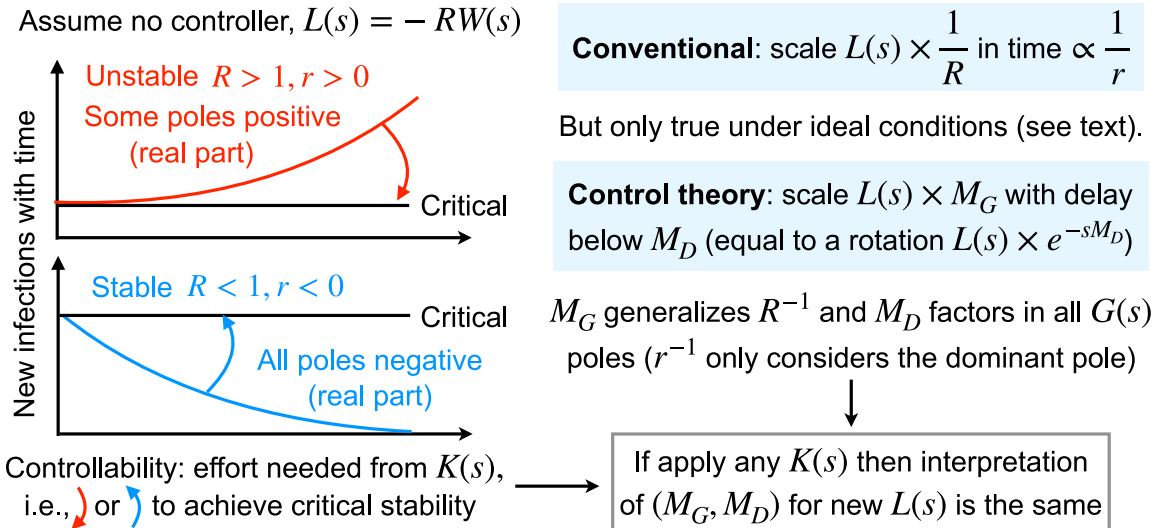
FIG. 1. Epidemic architecture and controllability definition. Panel (a) shows that the renewal epidemic model is a positive feedback system with signals being successively fed back along a loop and added to imported infections $M(s)$. The loop TF $L(s)$ (negative by convention for positive feedback) governs the poles of the closed-loop TF $G(s)$, which completely expresses how imports combine with the epidemic dynamics to generate new infections $I(s)$. When we intervene or initiate control action, we disrupt the feedback loop via a controller $K(s)$. Panel (b) explains the concept of controllability. This is the effort needed to drive the epidemic to critical stability where at least one pole has a 0 real part (others must be negative). We sketch stable and unstable epidemics with no controller and an initial import and contrast the conventional notion of controllability with our control theoretic approach. Our margin pair completely and precisely describes how $L(s)$ can be forced to criticality in the complex plane (via scaling and rotation) and, crucially, emphasizes that the distance of $L(s)$ from -1 measures controllability. The distances of r from 0 and R from 1 are specializations of this condition.

control actions that disrupt this loop. This reframing of the disease transmission process allows us to adapt tools from control theory [17] and derive what we term as the epidemic transfer function. This captures how incident (new) infections are generated under arbitrary generation time distributions and (linear) control actions in response to imported infection time series. We propose a rigorous controllability measure defined by the gain and delay margins of the epidemic transfer function, which quantify two important and distinct distances from the critical stability point [see Fig. 1(b)]. If an intervention is applied to two outbreaks, for example, the one with the larger pair of margins is more controllable under that intervention.

The gain margin M_G is the factor by which we can scale infections (known as the gain) before critical stability is attained, with $M_G = 1$ demarcating critical stability [18]. An $M_G = 2$ means the epidemic remains controlled unless infections double (e.g., from releasing interventions or the emergence of more pathogenic variants), while $M_G = 1/2$ means we must halve infections (e.g., via more stringent interventions that reduce contact rates) to control transmission. The delay margin M_D quantifies the lag we can afford when imposing interventions, with $M_D = 0$ delimiting critical stability [18]. An $M_D = 7$ indicates that if we take more than a week to intervene (e.g., to trace and isolate infected individuals), then we are unable to keep the epidemic controlled. This (M_G, M_D) pair framework yields a number of advantages and controllability results.

First, our margins more accurately describe what R and r only attempt to quantify —the scale and speed of the required control effort. Particularly, we show that the universal $1/R$ interpretation of controllability is only valid if interventions reduce infections without inducing dynamics and are implemented without delay. Under those conditions $M_G = 1/R$, and M_D is unimportant (i.e., it is undefined if $R > 1$ or infinite if $R < 1$). However, these conditions are unrealistic given mounting evidence that interventions change generation time and other epidemiological distributions (which is how a control action induces dynamics) and that practical constraints on outbreak control inevitably cause lags [7,19–22]. Additionally, by interrogating our epidemic transfer function, we find that r only quantifies the asymptotic epidemic growth rate [23] and so neglects short-term dynamics (which are crucial for understanding unwanted oscillations in infections) and their interactions with imposed interventions. These effects belie our conventional notions of controllability.

Second, our margin-based framework generalizes and unifies earlier approaches [1,8]. We characterize how presymptomatic spread, transmission heterogeneities from superspreading, multitype epidemics (but without considering contact structures), or cocirculating variants and surveillance limitations (e.g., reporting delays and underreporting) all modulate controllability. These complexities can be commonly evaluated using our two margins, which always have the same interpretation. This is beneficial because R or r is not always clearly defined or even meaningful for some of these complexities [24,25]. Importantly, our margins yield thresholds of controllability under these complexities that can be directly compared to decide the relative effectiveness of targeted and population-level interventions. These thresholds reduce to more conventional $1–1/R$-type results under the restrictive conditions mentioned above.

Last, our margins offer a more complete measure of controllability. Because induced dynamics from interventions, implementation delays, and surveillance imperfections are pervasive, even if proposed interventions are expected to drive $R < 1$ or $r < 0$, this does not reliably inform us about the required control effort and the robustness of the epidemic once controlled by these actions. We find ample evidence of controlled ($R < 1$) epidemics with $M_G < 1/R$, indicating that standard controllability interpretations overestimate robustness to increases in infections. We also show that some of these controlled epidemics possess $M_D = 7$–14 days, signifying that if the combined lag from surveillance and intervention delays rises above this value (e.g., due to downscaling of surveillance or control programs), then the epidemic will become destabilized. Neither r nor R can generally expose these issues. Our methodology probes the notion of controllability and raises questions about the understudied rebound effects of interventions.

II. METHODS

A. Renewal models and transfer functions

The renewal branching process [26] is a fundamental and popular infectious disease model that has been applied to describe epidemics of COVID-19, pandemic influenza, Ebola virus disease, measles, SARS, and many others [12,27]. This model defines how incident infections at time t, $i(t)$ depend on the reproduction number R and incidence at earlier times $i(\tau)$ ($\tau \leq t$, with a limit infinitesimally before t) via the autoregressive relationship in the left of Eq. (1),

$$i(t) = m(t) + R \int_0^t i(\tau)w(t - \tau)\mathrm{d}\tau,$$

$$I(s) = \frac{1}{1 - RW(s)} M(s). \tag{1}$$

We assume that R is constant during our period of interest. As Eq. (1) has no interventions and we consider initial epidemic stages, R is the basic reproduction number. Note that R can describe other (constant) effective reproduction numbers when the renewal process is a good approximation to later epidemic stage dynamics. Because this model is linear, we neglect nonlinear effects such as those due to the depletion of individuals that are susceptible to infection.

Equation (1) includes input infections $m(t)$ that have been imported or introduced into our region of interest and which eventually contribute to onward transmission [28]. Our output is $i(t)$. The kernel of the renewal autoregression is $w(t - \tau)$, which is the probability of an infection being transmitted after a duration of $t - \tau$ time units. The set of coefficients $\{w(\kappa), \kappa \geq 0\}$ composes the generation time distribution of the disease [15]. This captures variability in the time it takes for a primary infection to cause a secondary one. The generation time distribution is a key characteristic of a pathogen that determines the temporal aspects of its spread via the convolution in Eq. (1). We denote the mean generation time as $g = \int_0^\infty \tau w(\tau) d\tau$.

Since Eq. (1) is a linear model, we can analyze it in the frequency or s domain using Laplace transforms; e.g., $I(s) \stackrel{\text{def}}{=} \int_0^\infty i(t) e^{-st} dt$ is the transform of $i(t)$. This gives the right side of Eq. (1) after some algebra with capitalized forms as the transformed version of variables from the time domain. We visualize this using the block diagram of Fig. 1(a). We propose the ratio $G(s) = I(s)M(s)^{-1}$ as the epidemic transfer function (TF) that maps input importations onto output infections. The roots of its characteristic polynomial $1 - RW(s)$ [the denominator of $G(s)$] are the poles of the renewal process and completely define the stability of the epidemic [17]. A stable epidemic (infections decay with time given initial imports) has poles with negative real parts. An unstable epidemic (infections grow) has at least one pole with positive real part. Critical stability requires at least one pole with real part of 0, with all others negative.

The form of the characteristic polynomial of $G(s)$ confirms that the dynamics of the epidemic depend explicitly on R and the generation time distribution. These are two of three quantities commonly used to depict the transmissibility of infectious diseases. The third is the asymptotic exponential growth rate of infections $r = \lim_{t \to \infty} d \log i(t)/dt$ and also emerges from Eq. (1). Since $W(-s)$ is equivalent to the moment generating function of the generation time distribution evaluated at s, we know from Ref. [15] that $W(r) = R^{-1}$. Interestingly, r is also the dominant pole of $G(s)$. Often the growth rate is expressed as $t_c = \log \sqrt[r]{c}$, the time it takes for infections to (asymptotically) grow (or decline) by a factor c. At $c = 2$ we get the popular epidemic doubling time. We compute appropriate forms of $G(s)$ and its poles for generalizations of Eq. (1) that model various interventions under practical constraints in Sec. III.

B. Generation time distributions and Laplace transforms

The dynamics of infectious diseases are largely determined by the generation time distribution because $W(s)$ is the only nonconstant term in the TF of Eq. (1). We model $W(s)$ as a phase-type distribution, which is an expansive class built from combinations and convolutions of exponential distributions. This class can approximate any distribution [29] and includes the Erlang, exponential, deterministic (degenerate), and bimodal distributions that we examine in Sec. III. Erlang (or related gamma), deterministic, and exponential distributions are used to model influenza, measles, and COVID-19, among others [3,15,26,27]. Multimodal and mixture distributions are applied to diseases featuring multiple stages (which may even involve vectors) or pathways of transmission, such as malaria and Ebola virus disease [19,30].

All phase-type distributions conform to the relations in Eq. (2), where we use bold to denote vectors or matrices and x' to denote the transpose of some row vector x,

$$W(s) = \alpha(sI - T)^{-1}(-T1'), \qquad W(0) = \alpha 1' = 1. \quad (2)$$

In Eq. (2), $\mathbf{T}$ is a n^2 matrix of transition rates among the n distribution states, $\mathbf{I}$ the n^2 identity matrix, $\boldsymbol{\alpha}$ is a row vector of length n summing to 1 (providing weights to the states), and 1 is a row vector of n ones. Here, n represents the complexity of the phase-type distribution relative to how exponential distributions are combined. A standard exponential distribution has $n = 1$. Mixtures of phase-type distributions are also phase type, and we observe that their Laplace transforms evaluate to 1 at $s = 0$ (equivalent to the fact that probability distributions integrate to 1). We find that this basic property is important for computing controllability later in Sec. III.

For a mean generation time g, we can construct an Erlang distribution with shape a and scale b such that $g = ab$ by setting $n = a$, $\alpha = [1, 0, ..., 0]$, and $\mathbf{T}$ as a matrix with nonzero elements of $\mathbf{T}_{\kappa\kappa} = -b^{-1}$ and $\mathbf{T}_{\kappa\kappa+1} = b^{-1}$ for $1 \leq \kappa \leq n$. As a result, we obtain $W(s)$ as

$$W(s) = \frac{1}{(bs+1)^a}, \quad 1 - RW(s) = \frac{(bs+1)^a - R}{(bs+1)^a}. \quad (3)$$

We also find the characteristic polynomial or denominator from Eq. (1). This has roots when $s = b^{-1}(\sqrt[a]{R} - 1)$, which is the formula for the growth rate as expected from Ref. [15]. Exponential and deterministic distributions have $a = 1$ and $a \to \infty$, respectively. We get the roots of the characteristic polynomial of the exponential distribution by simply substituting in Eq. (3). The deterministic distribution yields $W(s) = e^{-sg}$ at the limit, is equivalent to applying a delay of g time units, and has a solution to its characteristic polynomial of $s = \log \sqrt[g]{R}$.

The bimodal distribution we consider is a mixture of two Erlang distributions with state sizes $n_1 = a_1$ and $n_2 = a_2$ and $\alpha = [\alpha_1, 0, ..., 0, 1 - \alpha_1, 0, ..., 0]$, which has $n_1 - 1$ and then $n_2 - 1$ zeros, respectively. The choice of α_1 defines the mixture weighting. The state matrix has size $(n_1 + n_2)^2$ with $\mathbf{T}_{\kappa\kappa} = -b_1^{-1}$ and $\mathbf{T}_{\kappa\kappa+1} = b_1^{-1}$ for $1 \leq \kappa \leq n_1$ and $\mathbf{T}_{\kappa\kappa} = -b_2^{-1}$ and $\mathbf{T}_{\kappa\kappa+1} = b_2^{-1}$ for $n_1 + 1 \leq \kappa \leq n_2$.

The b_1 and b_2 are chosen to get mean generation time g. We obtain $W(s) = \sum_{\kappa=1}^{2} \alpha_\kappa (b_\kappa s + 1)^{-a_\kappa}$ and numerically compute the roots of its characteristic polynomial. We can easily extend this formulation to allow higher-order mixtures. The phase-type structure allows us to describe complex distributions without losing analytical tractability.

C. Margins of stability and notions of controllability

In the above subsections, we described the elements of the renewal epidemic model and its characteristic polynomial $1 - RW(s)$. Here we review the concepts of gain, phase, and delay margin from classical control theory, which underpin our results and provide measures of how distant linear systems are from critical stability [17]. The loop TF $L(s) = -RW(s)$ (under no control) captures the dynamics around the loop as in the block diagram of Fig. 1(a). While in Sec. III we expand this $L(s)$ formulation to include a controller $K(s)$ that describes our epidemic intervention and investigate more generalized model architectures, the principles and interpretation that we detail here remain valid for all of these complexities.

Using $L(s)$ our characteristic polynomial becomes $1 + L(s)$ with the epidemic TF as $G(s) = [1 + L(s)]^{-1}$. Poles are complex solutions to $L(s) = -1 + j0$ where $j = \sqrt{-1}$. We can write a pole as the complex number $\sigma + j\omega$. At the critical stability point the dominant pole has $\sigma = 0$ so that $L(j\omega) = -1$. Control theory [17] states that the distance in the complex plane of $L(j\omega)$ from -1 reflects the stability properties of the process. We can describe this distance by the multiplicative factor (the gain), and the angular change (the phase) that, respectively, scale and rotate $L(j\omega)$ onto $-1 + j0$ in the complex plane. These distances are known as the gain and phase margin [17] and relate to polar descriptions of complex numbers. Note that the other poles also contribute to the form of $L(j\omega)$ and so influence the margins.

The gain margin $M_G \overset{\text{def}}{=} |L(j\omega_{\text{PC}})|^{-1}$ is the inverse of the magnitude of $L(s)$ evaluated at ω_{PC}, the first frequency at which the phase crosses $-\pi$ radians. Here, $|.|$ denotes magnitude so $|\sigma + j\omega| \overset{\text{def}}{=} \sqrt{\sigma^2 + \omega^2}$. The phase margin $M_P \overset{\text{def}}{=} \pi + \Phi[(L(j\omega_{\text{GC}})]$ is π plus the phase $\Phi[.]$ (in radians) evaluated at ω_{GC}, the frequency where $|L(j\omega)|$ first crosses 1 from above (known as gain crossover). The phase margin measures how much the phase lag (i.e., clockwise rotation in the complex plane) can be added to $L(j\omega_{\text{GC}})$ before driving the epidemic to critical stability [31,32]. The phase margin is not intuitive for our analyses but can be transformed into a more interpretable delay margin M_D (e.g., in some cases $M_D = M_P \omega_{\text{GC}}^{-1}$ [31]). This margin quantifies how much pure time delay or lag forces $L(s)$ to the critical point (lag reduces phase).

We compute both margins using in-built functions [specifically, allmargin(.)] from the MATLAB control system toolbox (see Ref. [33]). This essentially evaluates the magnitude and phase of $L(s)$ at every $s = j\omega$ and finds the appropriate crossover frequencies for determining the margins. When systems have multiple ω_{PC} or ω_{GC} crossover frequencies, we consider the minimum margin to ensure our characterization is robust. The gain and delay margins define the two ways (scaling and rotation) that we can drive our epidemic to critical stability. If we multiply $L(s)$ by the scale factor M_G or the angular shift e^{-sM_D}, which is the Laplace transform of a pure delay of M_D time units, we drive the epidemic to the critical stability point [32]. We compare this interpretation to more conventional epidemic measures in Fig. 1(b).

Importantly, the distance of our system from stability requires specifying both the gain margin and the delay margin [17]. We propose this pair representation as our measure of epidemic controllability, which quantifies the intervention effort required to control an unstable epidemic or the perturbation (e.g., to disease transmissibility R) required to destabilize an epidemic that is already under control. We expand this definition to include various model architectures and interventions in Sec. III. Note that in control theory, a system is only formally controllable if inputs exist that drive it from any initial state to any desired state in finite time. Our definition is more relaxed and considers only what changes force epidemics to critical stability and the required intensity of those changes. This relates to margins (also termed relative stability) and aligns with the informal definition commonly applied in infectious diseases [1,10].

Although controllability here defines the control effort needed to stabilize infections, it does not measure performance. Performance depends on our control objectives, i.e., what we want our interventions to achieve [17]. These may include desired margins but generally we may want our system response, $i(t)$ in this setting, to meet some desired dynamics $u(t)$. A key long-term performance metric is the error $\lim_{t \to \infty}[i(t) - u(t)] = \lim_{s \to 0} s[I(s) - U(s)]$. The second limit follows from the final value theorem [17]. If $U(s) = us^{-1}$ is a desired equilibrium of infections (us^{-1} is the Laplace transform of a step function with amplitude u), then $\lim_{s \to 0} sG(s)M(s) - u$ measures accuracy. Important short-term performance measures are the peak overshoot $\max_t[i(t) - u(t)]$ and the level of oscillation of $i(t)$ about either $u(t)$ or the equilibrium.

III. RESULTS

We start by expanding the framework from Sec. II to explore the standard assumption that larger R or r signals a less controllable epidemic [1,10,33]. This belief is sensible as increases in R cause infections to multiply more and rises in r engender faster multiplication. In Fig. 1(b), we recap these conventional notions of controllability. We prove that these universal notions are only true under restrictive and idealistic intervention assumptions. Extending the margins above, we construct a rigorous measure of epidemic

controllability that accurately reflects the control effort needed to stabilize a growing epidemic and the robustness to perturbations of a controlled epidemic. To maintain analytic tractability and as we focus on deriving fundamental insight into controllability, we study constant R or r and neglect stochasticity (see Sec. II). In later sections, we discuss relaxations of these assumptions and show that our framework can assess how variant dynamics, presymptomatic spread, superspreading, intervention lags, and surveillance biases all modulate controllability.

A. Epidemic models, feedback control, and transfer functions

The renewal process is widely used to model acute infectious diseases and is given in Eq. (1). There, new or output infections at time t, $i(t)$ result from multiplying all active infections by R with $m(t)$ as the introduced infections or input. Past infections are active if they can still transmit. The generation time distribution $\{w(\kappa), \kappa \geq 0\}$ sets the transmission probabilities [26,27] with the active infections computed as a convolution $\int_0^t w(t - \tau) i(\tau) d\tau$. However, these quantities from Eq. (1) describe uncontrolled dynamics. Here we extend this model to include control. We define a generic control strategy as one reducing infections to $\lambda(\tau) \leq i(\tau)$ so that $\int_0^t w(t - \tau)\lambda(\tau) d\tau$ is the equivalent convolution. This yields

$$i(t) = m(t) + R \int_0^t \lambda(\tau) w(t - \tau) d\tau,$$
$$\lambda(t) = \int_0^t i(\tau) k(t - \tau) d\tau. \qquad (4)$$

The controller achieves this reduction by weighting past infections by a kernel $k(\tau)$ with overall effect $\int_0^\infty k(\tau) d\tau = k$. If this kernel has mass only at the present so $k(t) = k\delta(t)$, with $\delta(t)$ as the Dirac delta function, we get constant (memoryless) feedback control and $\lambda(t) = ki(t)$. Generally, $0 \leq k \leq 1$ as control reduces infections. However, if the epidemic is already stable, we may set $k > 1$ to assess robustness to perturbations in infections; i.e., we want to find the largest k that achieves critical stability. The expressions in Eq. (4) become the standard ones of Eq. (1) by removing control; i.e., by using a constant controller with overall effect $k = 1$.

We Laplace transform Eq. (4) (see Sec. II) with $I(s)$, $M(s)$, and $W(s)$ as the transformed infection incidence, importations, and generation time distribution in the frequency or s domain. Since convolutions are products in this domain, the controller satisfies $\Lambda(s) = K(s)I(s)$ with $K(s)$ as its transform. We represent these operations as the block diagram in Fig. 1(a), where we identify that, fundamentally, an epidemic involves a positive feedback loop between past and upcoming infections. Taking the product of blocks along the loop, we obtain the loop TF as $L(s)$ in Eq. (5) below. Control aims to disrupt this loop,

$$L(s) = -K(s)RW(s), \qquad G(s) = \frac{1}{1 - K(s)RW(s)}. \qquad (5)$$

Using this structure, we can define the transmission dynamics by the properties of the closed-loop TF $G(s) = I(s)M(s)^{-1}$, which describes how imports drive total incidence. We can see the importance of $L(s)$ by noting that $G(s) = [1 + L(s)]^{-1}$ [18]. The poles of $G(s)$ determine the dynamics and stability of the epidemic and are complex number solutions of $L(s) = -1 + j0$ (see Sec. II). We recover the uncontrolled epidemic TFs by setting $K(s) = 1$, which is the Laplace transform of the constant controller above with $k = 1$.

We can interpret Eq. (5) by recognizing that an unstable epidemic [at least one pole of $G(s)$ has a positive real part] successively multiplies infections along the loop. This constitutes the positive feedback we illustrate in Fig. 1(a). Interventions or control actions having magnitude $|K(s)| < 1$ limit this positive feedback by interfering with the loop and hence attenuating this multiplication. Modification of the intrinsic epidemic dynamics $RW(s)$ by the controller $K(s)$ within the loop achieves this goal. A stable epidemic [all poles of $G(s)$ have nonpositive real parts] is also multiplicative, but infections reduce along the loop. We can apply $|K(s)| > 1$ as an amplifier of infections to study the robustness of the controlled epidemic to any destabilizing perturbations or uncertainties (e.g., surges in transmissibility or more pathogenic variants).

There are two important corollaries of Eq. (5). First, the poles of the epidemic TF $G(s)$ are the roots of the characteristic polynomial $1 - K(s)RW(s)$. Solving this (see Sec. II), we find the epidemic growth rate r is the dominant pole; i.e., it is the major contributor to the dynamics of the system (see Sec. II for the explicit calculation in the uncontrolled case), and its variations reflect the impact of the controller $K(s)$. Second, $K(s)$ directly regulates both the generation times and R. For constant controller $K(s) = k$, the epidemic has an effective reproduction number of kR, with related changes to its effective growth rate. These observations seemingly support the common paradigm of modeling interventions and assessing controllability directly from how R or r (or related parameters such as doubling times or infectiousness) change [12].

B. A framework for investigating epidemic controllability

The above corollaries actually expose why these parameters are insufficient for defining controllability, i.e., the effort required to stabilize an unstable epidemic, or the intensity of the perturbations required to destabilize a stable

epidemic. Specifically, the difficulty of controlling the epidemic in real time also depends on its other poles (which may be oscillatory) [18], and only asymptotically are infections completely determined by the dominant pole r. Additionally, the assumption that $K(s)$ is constant and introduces no dynamics is unrealistic (e.g., isolation is known to reduce generation times [20,21]) and only likely true in very limited circumstances. We therefore need to account for transient and intervention-induced dynamics [23,34].

To investigate the implications of these corollaries, we propose a new framework for defining epidemic controllability, which adapts classical control theory as well as generalizes and more rigorously quantifies the interpretation frequently ascribed to R or r. Figure 1(b) summarizes and contrasts this framework to standard (albeit implicit) notions of controllability. We know from Eq. (5) and stability theory [17] that as $L(s)$ approaches $-1 + j0$ in the complex plane, the closed-loop $G(s)$ becomes critically stable; i.e., it is on the verge of instability with $r = 0$. The gain M_G and delay M_D margins [18] precisely determine the distance of $L(s)$ from $-1 + j0$ (see Sec. II for how to compute these and related margins) [17].

For stable epidemics [$r < 0$; i.e., all $G(s)$ poles are in the left half of the complex plane], M_G and M_D, respectively, measure how much we can scale up or delay infections before the system becomes critical [32]. Accordingly, for unstable epidemics [$r > 0$; i.e., at least one $G(s)$ pole is in the right half plane], they quantify how much we must scale down or limit delay to stabilize an epidemic (assuming certain conditions [17]). If an epidemic admits a margin pair (M_D, M_G), then we can multiply $L(s)$ along its loop by e^{-sM_D} or M_G, respectively to force the epidemic to its critical stability point. Critical stability is rigorously defined as when $K(s) = 1$ in Eq. (5), then r matches $R - 1$ in sign and is the dominant $G(s)$ pole so $L(s) = -1$, $R = 1$, and $r = 0$ all correspond. There is an analogous association with the effective R and r when some control is acting [$K(s) \neq 1$]. The crucial distinction we make is that the distance of $L(s)$ from -1 and not that of R from 1 or r from 0 is what actually determines controllability.

The margins we propose to measure this distance precisely and holistically characterize the essence of earlier notions of control effort by quantifying the magnitude and time by which we must alter infections to attain the brink of stability. Stable or controlled epidemics feature $M_G > 1$ and $M_D > 0$, and larger margins signify better controllability [see Fig. 1(b)]. Computing these for Eq. (5), we get $M_G = |-K(j\omega_{PC})RW(j\omega_{PC})|^{-1}$ [17] where ω_{PC} is the phase crossover frequency (see Sec. II). From the properties of distributions, $W(0) = 1$. We confirm this in Sec. II for a universal class of phase-type generation time distributions [29] that include realistic models of $w(t)$ for many

infectious diseases [15,27]. Accordingly, when $\omega_{PC} = 0$, $M_G = |-K(0)R|^{-1}$. As critical stability occurs when $M_G = 1$, the critical control effort required, based on this gain margin, is therefore $K^* = |K(0)| = R^{-1}$.

We show in Fig. 2 for constant controllers applied to epidemics with various generation time distribution shapes [Fig. 2(a)] that $\omega_{PC} = 0$ is true and unique. For stable epidemics, we find $M_D \to \infty$ (not shown; see Ref. [33]). Consequently, under these conditions, controllability is completely established by the magnitude of R^{-1} [Fig. 2(c)], which correlates well with the Euclidean distance in the complex plane between $L(s)$ and -1 (inset). When the epidemic is unstable, the gain margin is also set by R^{-1}, but there may be ways of removing system lag that also define a dimension of control. However, if we apply a constant controller (so system lag does not change) with $k = \alpha R^{-1}$ and $\alpha < 1$, the controlled epidemic has an effective reproduction number of α and hence a controllability of α^{-1}.

The dominant pole and hence the effective growth rate also shifts from being the solution of $RW(s) = 1$ to that of $(kR)W(s) = 1$. As this equation is scaled only, the growth rate is now related to the effective reproduction number kR. For gamma distribution generation times with parameters (a, b) for example (see Sec. II), the growth rate changes from $b^{-1}(\sqrt[a]{R} - 1)$ to $b^{-1}(\sqrt[a]{kR} - 1)$ [15]. Consequently, if $\omega_{PC} = 0$, we can completely describe the controllability of an epidemic using the size of reproduction numbers or growth rates. As growth rates are asymptotic (i.e., other poles decay in impact as $t \to \infty$), we can equally describe controllability from widely used exponential growth models of the form $i(t) = i(0)e^{p_1 t}$, with p_1 as the dominant pole of this model. This closely matches (and often overlaps) the dominant pole p of the more complex renewal processes [Fig. 2(b)]. Note that epidemics with the same controllability may have diverse responses to imports and transient (short-term) dynamics [Fig. 2(d)].

Our framework therefore supports the conventional definition that larger R or r indicates lower controllability but reveals that this requires $\omega_{PC} = 0$ and that our controller is constant [i.e., we need $k(t) = k\delta(t)$]. Under these conditions, we cannot destabilize the epidemic through perturbations that add delay (or change phase). This holds for broad classes of phase-type generation time distributions. We show next that our more generalized controllability definitions are necessary because these settings are strongly restrictive and not likely to occur in practice; i.e., control actions frequently introduce dynamics (e.g., by modifying incubation periods, generation times, and infectiousness durations [21,22]). Further, we know that delays to interventions, surveillance biases, presymptomatic spread, and superspreading all impact controllability. We demonstrate that our definitions can rigorously unify these complexities.
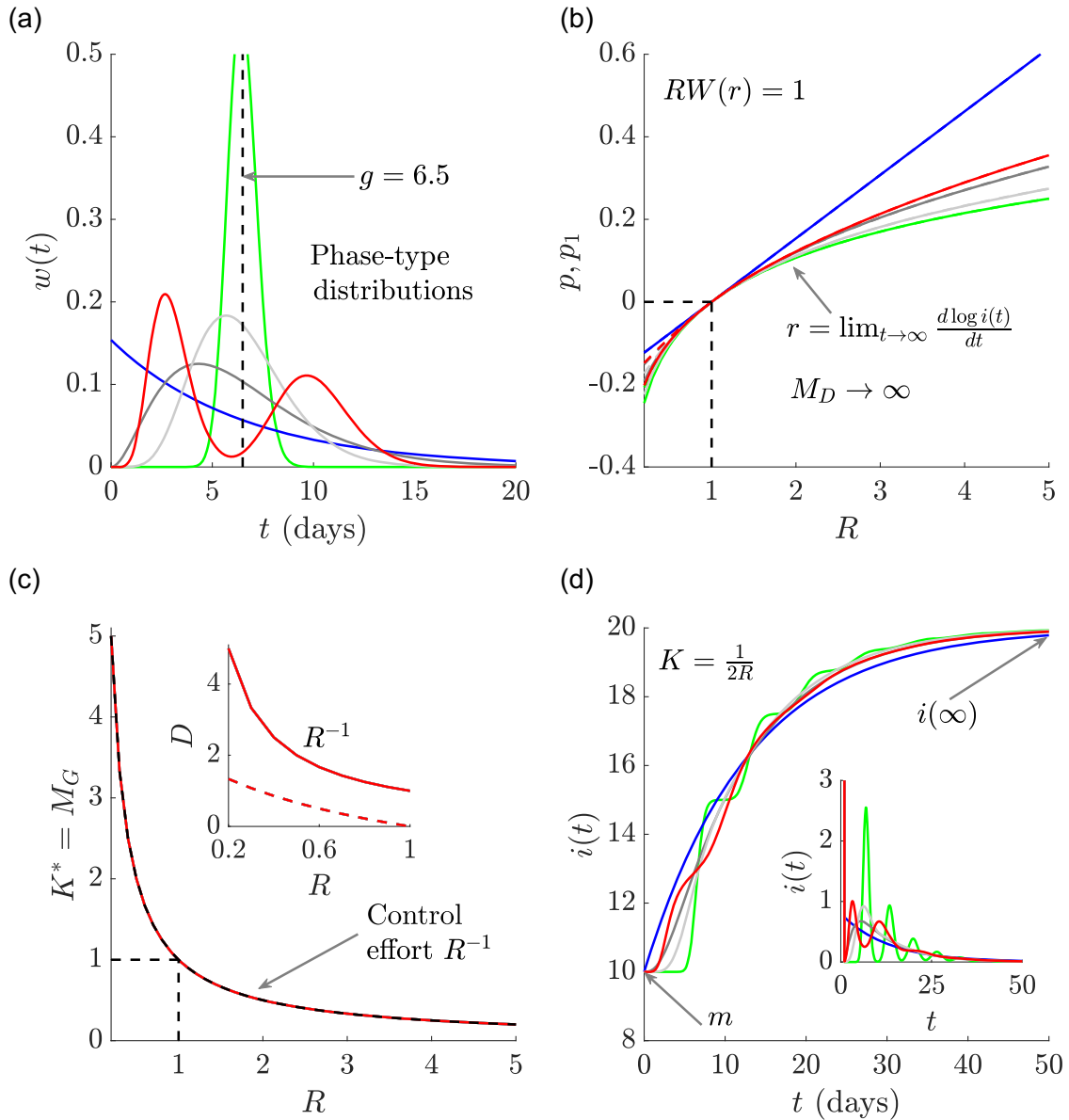
FIG. 2. Epidemic controllability under ideal conditions. We assess controllability via gain and delay margins for epidemics subject to constant (nondynamical) control $K(s) = k$ with phase crossover frequencies of 0 (see text). Panel (a) shows the generation time distributions $w(t)$ of simulated epidemics that we analyze, which have fixed mean generation time g (taken from COVID-19 [3]) but feature markedly different shapes. Panel (b) plots the growth rate r of these epidemics [colors match (a)], which is the dominant pole p (solid) of the resulting TFs $G(s)$. These closely match the dominant pole p_1 (dashed, often overlapping the solid line of the equivalent p) of an approximating epidemic featuring simple exponential growth $i(t) = i(0)e^{p_1 t}$. Panel (c) plots the gain margin M_G or critical controller K^* that drives the system to the brink of instability (the delay margin M_D here is infinite). The K^* curves from every $w(t)$ exactly equal R^{-1}. These curves correlate well with D (inset), the Euclidean distance between $L(s)$ and -1. Panel (d) demonstrates that although controllability is the same, transient dynamics of infections may differ (they also depend on nondominant system poles). We plot incident infections $i(t)$ in response to stable numbers (main) of imported infections ($m(t) = m$) and to a one-day pulse (inset) of m imports [colors match (a)].

C. Problems with existing controllability definitions

Previously, we established conditions under which our generalized framework for assessing controllability reduced to the popular but informal definition applied in epidemiology. However, the conditions that allow this interpretation are strongly restrictive for two reasons. First, the only controller guaranteed to satisfy $|K(0)| = R^{-1}$ and have unique $\omega_{PC} = 0$ is the constant $K(s) = k$. This controller seems unrealistic given that interventions not only scale infections but also change the distribution of
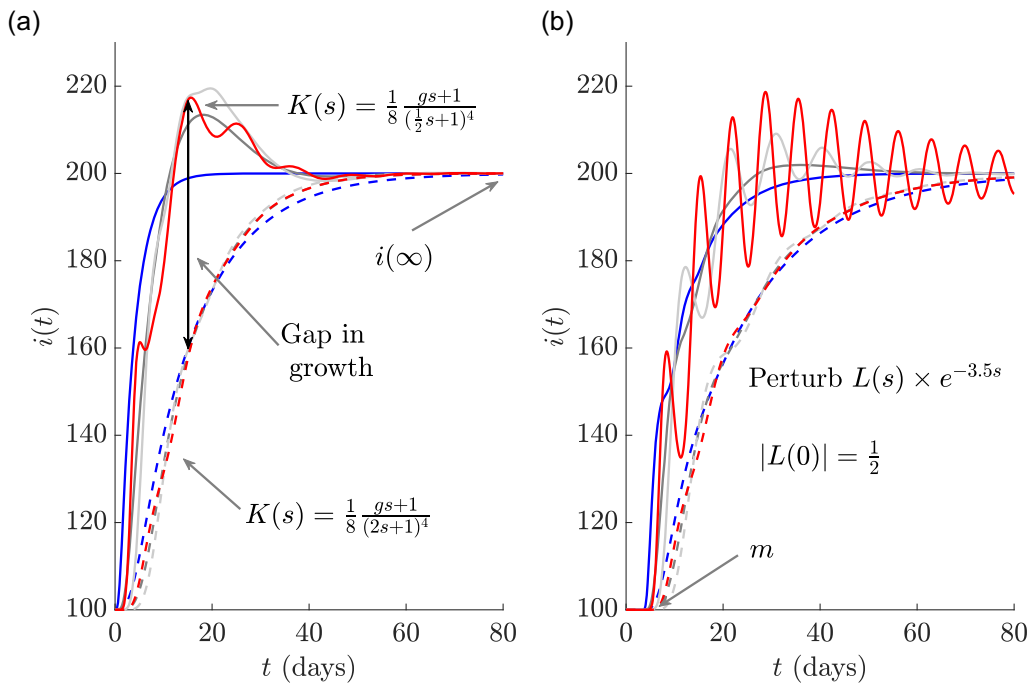
FIG. 3.　Controllers introducing additional dynamics. We simulate epidemics that are forced by a constant supply of imported infections $[m(t) = 100]$. Panel (a) shows the resulting curves of incidence for epidemics with generation time distributions from Fig. 2 (excluding the green one because this becomes unstable; curves match in color) when nonconstant control $K(s)$ is applied. There are major discrepancies among responses to interventions (controllers) that induce substantial dynamics (solid) and those behaving as we would conventionally expect (dashed). The former show salient transients that disrupt controllability and feature finite delay M_D (and in some cases, $M_G < 2$). Conventional interpretations expect $M_G = 2$, $M_D \to \infty$. The long-term incidence $i(\infty)$ remains, however, unchanged for all our controllers. In panel (b) we apply a 3.5-day delay ($e^{-3.5s}$ in the s domain). This pushes the curve from (a) with finite $M_D \approx 4.2$ days toward instability. The value of a two-margin description is clear.

generation times and other epidemiological quantities and hence induce additional dynamics [and poles in $G(s)$] [20–22]. Any realistic intervention (e.g., social distancing or contact tracing) likely scales infections and slows them from occurring.

We demonstrate this for the generation time distributions in Fig. 2(a) using controllers of form $K(s) = \frac{1}{8}(1 + gs)/(1 + bs)^a$, which induce minimal dynamics and satisfy $\int_0^\infty k(\tau)d\tau = k$. Here, $K(s)$ can model interventions that change the effective reproduction number as well as the generation times of the epidemic. For example, if the uncontrolled epidemic has exponentially distributed $w(t)$ with mean g, then $W(s) = 1/(1 + gs)$ and the loop TF changes from $-R/(1 + gs)$ to $-(R/8)(1 + bs)^a$; i.e., the control scaled down infections by a factor of 8 and forced the mean generation time to ab. This illustrates how controllers can realistically alter dynamics. Intervention-driven changes to generation times have been observed for malaria, COVID-19, and other diseases [19,20].

When $K(s)$ is applied to epidemics with $R = 4$, if $\omega_{\text{PC}} = 0$, then $M_G = |-K(0)R|^{-1} = 2$. This controller is strongly stabilizing (we can double infections before critical stability), attenuating infections so that the effective reproduction number of the controlled epidemic is $\frac{1}{2}$.

However, this standard interpretation is misleading and incomplete due to the temporal variations that control actions may introduce. In Fig. 3(a), we compare the resulting epidemic trajectories under two $K(s)$ examples. For the first ($b = 2, a = 4$), the gain and delay margins together with the response to a stable input of $m(t) = 100$ infections over time is consistent with Fig. 2. Note that the g and R we use here are among the values estimated for COVID-19.

Strikingly, for the second case ($b = \frac{1}{2}, a = 4$), the response is markedly different, featuring oscillations and faster (transient) growth that might initially strain available resources. The gain margin for these cases is still 2 (though in some instances it can fall below 2) but, importantly, the delay margin for one of the $w(t)$ in Fig. 2(a) becomes finite and small ($M_D \approx 4.2$ days). This effect is pronounced, and this $K(s)$ can cause the overall generation time to shrink to roughly two days. Case isolation was found to cause similar shrinking for COVID-19 [21]. Smaller M_D values can occur for further $w(t)$ types under more complex controllers (not shown). As much is unknown about these rebound effects of interventions [22], we cannot be certain about realistic formulas for $K(s)$. Recent works [35] emphasize the need for collecting the data types that will

allow precise $K(s)$ parametrization. When such data become available, our margins will be best placed to assess controllability and expose any unexpected rebound effects.

The finite delay margin is especially valuable, revealing that interactions between the epidemic and interventions can cause robustness losses. Real interventions always have latencies [13], making M_D crucial. If control is applied after a 3.5-day delay, we obtain infection curves as in Fig. 3(b). There we observe that the red curve approaches instability and realize that there is a hard limit from M_D on how late we can respond to an epidemic if we want control to work. The importance of delays in epidemic control is a known issue [9,16], but it is rarely factored into epidemic controllability directly. Our (M_D, M_G) framework is comprehensive and exposes the pitfalls of measuring controllability only in terms of R or r (while not shown, the dominant poles, and hence, r in Fig. 3 are similar for both the finite and infinite M_D scenarios).

The second major problem with conventional definitions of controllability is that they are not easily computed, interpreted, or compared when practicalities such as presymptomatic spread, superspreading, variant dynamics, and surveillance imperfections (e.g., reporting delays and incomplete case ascertainment) occur [1,24]. In the next two sections, we expand our models and demonstrate that the (M_D, M_G) framework presents a unified and interpretable approach to measuring and monitoring epidemic controllability under all of these complexities. No matter the specific model structure, the boundaries of controllability specified by our (M_D, M_G) pair are directly comparable and possess exactly the same interpretation as in Fig. 1.

D. Surveillance limitations and presymptomatic spread

Until now, we have assumed that we can observe and apply control to all new infections. This is unrealistic, as commonly we can only count cases or deaths, which are delayed and scaled versions of infections [36,37]. Here we generalize Eqs. (4) and (5) to include these effects. We denote the proportion of infections that we observe as cases by probability $0 \leq \rho \leq 1$ and model the latency in observing these cases with a distribution $h(t)$. Our controller acts on the incidence of cases $c(t)$, and $i(t) - c(t)$ infections remain unobserved. This yields

$$\lambda(t) = \int_0^t c(\tau)k(t - \tau)\mathrm{d}\tau,$$
$$c(t) = \rho \int_0^t i(\tau)h(t - \tau)\mathrm{d}\tau. \qquad (6)$$

The unobserved infections continue to propagate the epidemic as they remain uncontrolled. We therefore construct the combined renewal model

$$i(t) = m(t) + R\int_0^t (i(\tau) - c(\tau))w(t - \tau)\mathrm{d}\tau$$
$$+ R\int_0^t \lambda(\tau)w(t - \tau)\mathrm{d}\tau. \qquad (7)$$

This collapses into Eq. (4) when reporting is perfect; i.e., $\rho = 1$ and $h(t)$ has all its probability mass at the present $[h(t) = \delta(t)$, the Dirac delta] so that $c(t) = i(t)$.

We again take Laplace transforms of Eqs. (6) and (7) to obtain our key TFs for evaluating epidemic controllability in Eq. (8). We illustrate this architecture in Fig. 4(a) and observe that we also obtain TFs for the observed cases easily since $C(s)M(s)^{-1} = \rho H(s)G(s)$,

$$L(s) = -RW(s)\{1 - \rho H(s)[1 - K(s)]\},$$
$$G(s) = \frac{1}{1 + L(s)}. \qquad (8)$$

When $K(s) = 1$ in Eq. (8), we recover the uncontrolled epidemic TFs [see Eq. (1)]. Perfect surveillance means $\rho H(s) = 1$ and reverts Eq. (8) to Eq. (5). If we instead perform control on another proxy of infections, for example, deaths or hospitalizations, then ρ is the proportion of infections that lead to mortality or hospitalization (e.g., for the incidence of deaths, this includes the infection fatality ratio and the proportion of deaths that are observed). The distribution $h(t)$ then models the lag from becoming infected to mortality or being admitted to the hospital [37,38].

This formulation equally models presymptomatic and asymptomatic spread, with $h(t)$ defining the delay between infection and presenting symptoms and ρ as the proportion of infections that never become symptomatic. We compute our (M_D, M_G) pair to assess how these differing transmission and surveillance characteristics impact controllability. Equation (8) includes all the key controllability factors outlined in Ref. [1] and describes targeted interventions such as quarantine, contact tracing, or isolation but not wide-scale lockdowns (we control only the observed infections). Lockdowns and other nonselective interventions conform more closely to Eq. (5), as they act indiscriminately on all infections, including those that we never observe.

We know from earlier that critical stability is achieved when $L(s) = -1$. We substitute this into Eq. (8) and find that our control needs to satisfy the left side of Eq. (9). As a constant $K(s) = 0$ represents the maximum possible control effort (i.e., all observed infections are suppressed completely), we insert this condition and rearrange to derive the threshold on the right side of Eq. (9), outlining the requirements on the surveillance noise or level of presymptomatic spread for the epidemic to just be controllable. A smaller $|\rho H(s)|$ causes loss of controllability and provides evidence that wide-scale interventions or surveillance improvements are needed. The relations of

(a) Imperfect surveillance and presymptomatic spread

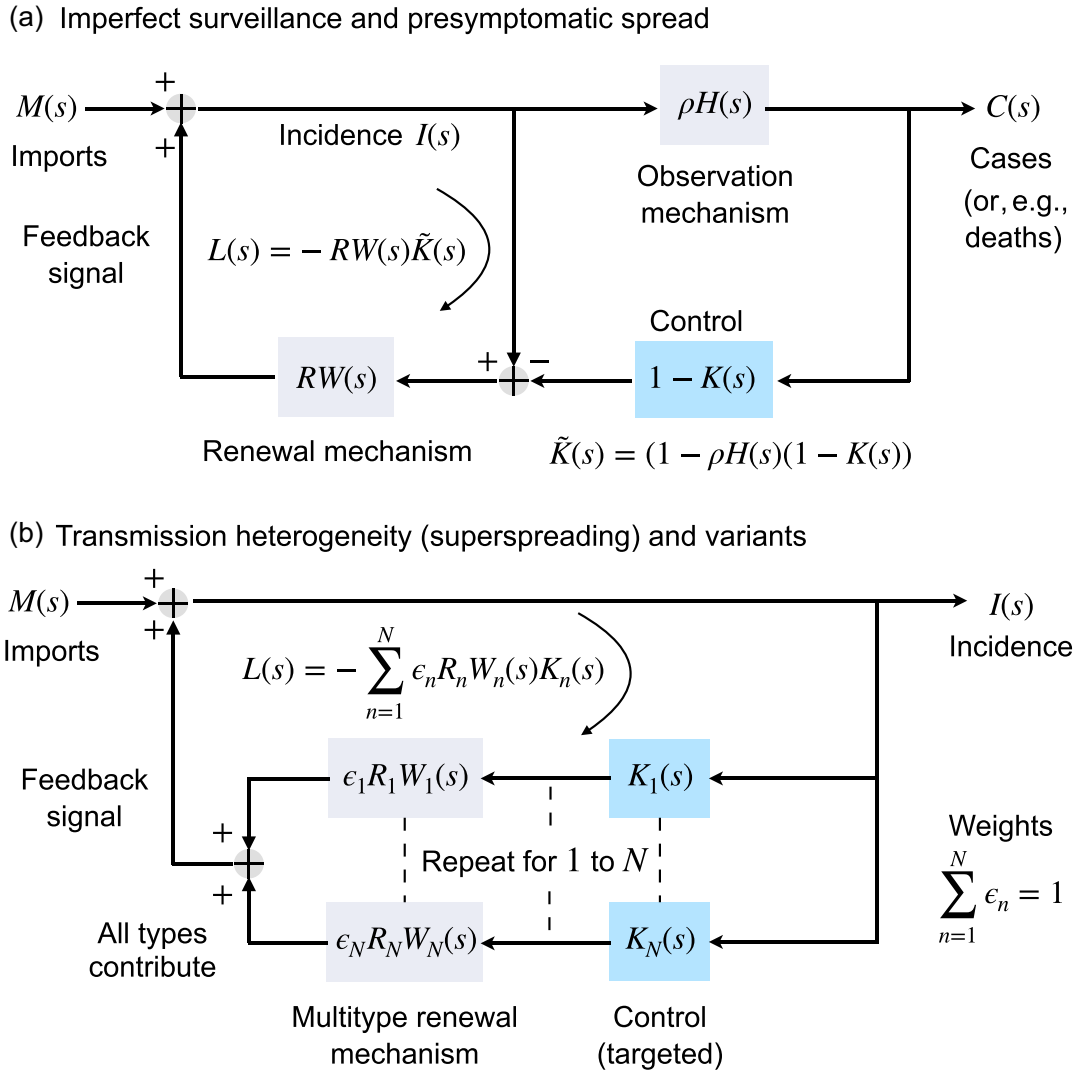### (b) Transmission heterogeneity (superspreading) and variants

FIG. 4.　Generalized controlled renewal model architectures. Panel (a) illustrates the block diagram of a renewal model for which only a portion of the new infections $I(s)$ are observable and hence can be controlled by $K(s)$. This portion $C(s)$ may model cases, deaths, or any other time series that is mediated by a scale factor ρ and a lag distribution $H(s)$. This architecture represents imperfect surveillance mechanisms or presymptomatic spread. Panel (b) shows the structure of a multitype, controlled renewal model describing N infectious types or stages with diverse reproduction numbers R_n and generation time distributions $W_n(s)$. The weight ϵ_n is the fraction of new infections of type n. This architecture models transmission heterogeneity including superspreading, cocirculating variants, and diseases with multiple routes for spread but considers the combined contributions of all types (hence, contact matrices are not needed). Both panels have closed-loop TFs $G(s) = I(s)M(s)^{-1} = [1 + L(s)]^{-1}$, with loop TF $L(s)$ as described. See main text for details on how $K(s)$ and the $K_n(s)$ define controllability.

Eq. (9) are required only to hold at the $s = j\omega$ satisfying $L(s) = -1$,

$$K(s) = 1 - \frac{1 - [RW(s)]^{-1}}{\rho H(s)}, \quad |\rho H(s)| \ge \left|1 - \frac{1}{RW(s)}\right|. \quad (9)$$

If $\omega_{\mathrm{PC}} = 0$, then this requirement is met at $\rho \ge 1 - R^{-1}$, as $W(0) = H(0) = 1$. This matches the critical contact tracing efficiency derived in Ref. [2] and the presymptomatic condition of Ref. [1] and confirms how our methodology generalizes more conventional notions of controllability (it also relates to the herd immunity threshold, though we do not consider this directly as our models neglect depletion of susceptibles). Equation (9) verifies that we need both margins because $\omega_{\mathrm{PC}} = 0$ is not guaranteed here, even if controllers are constant. The temporal impact of imperfect surveillance or presymptomatic spread via $H(s)$ means that the dynamics leading to situations as in Fig. 3 always exist. Transient dynamics are crucial and unavoidable.

We verify this point in Fig. 5, showing how controllability depends on ρ and $H(s)$. We first set $H(s) = 1$ and
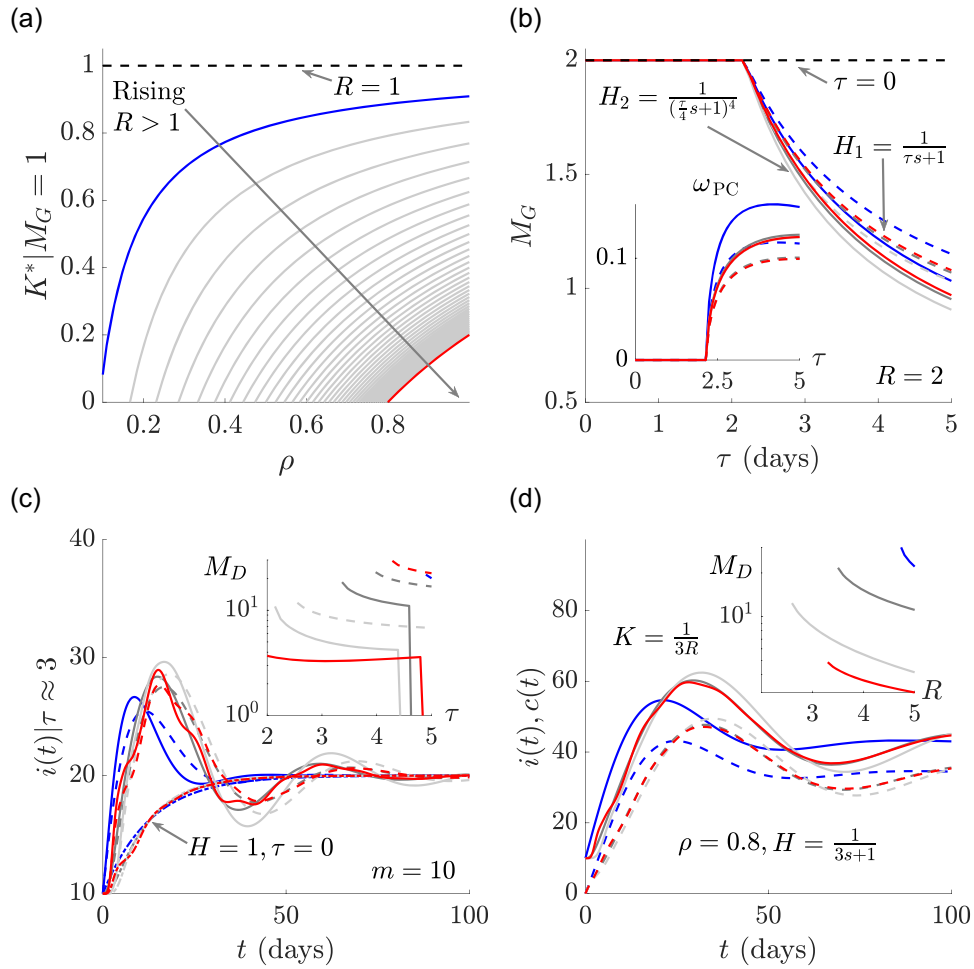
FIG. 5. Surveillance noise and presymptomatic spread. We investigate how imperfect case reporting, or equivalently, presymptomatic spread, limits the controllability of epidemics using our (M_D, M_G) framework. Panel (a) shows for curves of constant $R \geq 1$ (rising from blue to red, which is at $R = 5$) how the reporting rate or proportion of symptomatic infections ρ reduces controllability. Smaller ρ requires more control effort to attain critical stability, i.e., a smaller K^* is needed for a gain margin $M_G = 1$. There is no reporting delay or presymptomatic distribution in this analysis so $H(s) = 1$. Panel (b) sets $\rho = 1$ and investigates the influence of two $H(s)$ distributions, H_1 (dashed) and H_2 (solid) modeling exponential and gamma distributions. Both have mean lag τ, $R = 2$, and a controller applied that achieves $M_G = 2$ if the phase crossover frequency $\omega_{\text{PC}} = 0$. We find that as τ increases M_G falls below 2 indicating a decline in controllability. This results from ω_{PC} increasing above 0 (inset). Colors in this and panels (c) and (d) match the generation times modeled from Fig. 2(a) (excluding the green). Panel (c) confirms that $H(s)$ causes the delay margin M_D to become finite [inset, dashed or solid corresponding to (b)]. This reduced controllability is visible from the peaked, oscillatory response in new infections $i(t)$ for a constant number of imports $m(t)$ (main). This effect is similar to that in Fig. 3. Here, dot-dashed lines plot the response in the absence of $H(s)$ [i.e., setting $H(s) = 1$]. Panel (d) shows the combined influence of lags and underreporting given the constant controller of $K = 1/(3R)$. The inset demonstrates how M_D falls with R, and the main shows the infection (solid) and case $c(t)$ (dashed) epidemic curves in response to constant imports (colors match generation time distributions).

explore the controller gain needed to get $M_G = 1$, which sets critical stability. In the absence of underreporting, we have $\rho = 1$ and $K^* = R^{-1}$ for any R. Figure 5(a) shows that our required K^* substantially deteriorates, highlighting that we need additional control effort to stabilize the epidemic as ρ decreases. When $K^* = 0$, the epidemic is no longer controllable by these targeted interventions. If we cannot improve surveillance quality or equally diminish asymptomatic spread (so ρ rises), then population-level controls are warranted. Strikingly, at $R = 5$ (red), we cannot control the

epidemic unless more than 80% of all new infections are observed (sampled) or symptomatic. Equation (9) defines fundamental limits on controllability.

In Figs. 5(b) and 5(c), we assume perfect reporting and test the influence of delays in reporting, or equivalently, lags in infections becoming symptomatic. We investigate two $h(t)$ distributions $H_1(s)$ and $H_2(s)$ in the frequency domain, with results, respectively, as dashed or solid. These model exponential and gamma distributed delays with means τ. We apply controls that force $M_G = 2$ when

$\omega_{PC} = 0$ but find in Fig. 5(b) that our gain margin declines with τ. This occurs as $\omega_{PC} > 0$ (inset). Figure 5(c) further shows that the delay margin M_D becomes finite, decaying with τ (inset). Hence, $H(s)$ reduces both the scaling and delays that the controlled epidemic can robustly support. Incident infections $i(t)$ display oscillatory dynamics with substantial peaks (main). This contrasts the plots featuring no delay, i.e., $\tau = 0$ (dot-dashed). Colors indicate the $w(t)$ from Fig. 2(a) underlying the results in Figs. 5(b)–5(d).

On its own, $H(s)$ substantially reduces our controllability. At $\tau \geq 4$, we find that $M_D \to 0$ (and $M_G < 1$) signifying that the epidemic is now unstable. Epidemics with larger τ are necessarily uncontrollable. We combine both ρ and $H(s)$ in Fig. 5(d) but vary R and apply a strong controller that scales down cases by $1/(3R)$. Even for this constant control, we find a finite M_D that declines with R (inset) and large amplitude oscillations in $i(t)$ (solid, main). We also plot the observed cases $c(t)$ (dashed), which are the fraction of infections we can control. Both of the (M_D, M_G) pair are therefore critical to accurately quantifying epidemic controllability. In Fig. 5, the ranges of ρ and τ that we explore are realistic and even better than those often reported for countries with good COVID-19 surveillance, which can feature smaller ρ or larger τ [37,39,40].

E. Superspreading, variants, and multiple infector types

Our (M_D, M_G) framework can also evaluate the controllability of epidemics that are composed of multiple infectious types or transmission routes. This models superspreading, cocirculating variants, and pathogens with multiple pathways of spread. We unify these multitype epidemics using the renewal process of Eq. (10), which features N distinct types or pathways,

$$i(t) = m(t) + \sum_{n=1}^{N} R_n \int_0^t \lambda_n(\tau) w_n(t - \tau) d\tau,$$

$$\lambda_n(t) = \int_0^t \epsilon_n i(\tau) k_n(t - \tau) d\tau. \qquad (10)$$

We denote the reproduction number, generation time distribution, and controller of the nth type with subscript n. The parameters ϵ_n define the proportion of incidence associated with the nth type and $\sum_{n=1}^{N} \epsilon_n = 1$. By dividing control into N functions, we allow for type-specific control. This includes nontargeted control [all $k_n(\tau)$ are the same] and situations where some types are uncontrolled [those $k_n(\tau) = 1$], perhaps due to being unobservable.

Specializations of Eq. (10) can model superspreading or transmission heterogeneity (e.g., we set $N = 2$, $R_1 \gg R_2$, $\epsilon_1 = \frac{1}{5}$, and $\epsilon_2 = \frac{4}{5}$ to describe cases where 20% of new infections have substantially larger transmissibility, which aligns with data on many diseases [41]), pathogenic variants with differing transmissibility and generation times

[e.g., with N as the number of cocirculating variants, although we assume early growth so that the ϵ_n are fixed [42,43]], and diseases with diverse transmission pathways [e.g., Ebola virus disease has sexual and nonsexual pathways with distinct $w_n(t)$ [30]]. This construction may not always be valid, e.g., for cocirculating variants at other epidemic stages or where competition and selection imply that a specific variant eventually dominates. In these scenarios, ϵ_n and R_n are likely time varying, and our construction is only a constant approximation to these variations.

Relatedly, the above specializations do not include explicit interaction among types [though all types compose the total $i(t)$], as this commonly requires additional cross-type reproduction numbers and auxiliary data (e.g., to estimate contact matrices or to evaluate key epidemic thresholds) [44,45]. Such extensions are possible provided the interacting system can be framed as a multidimensional, linear renewal model. We do not consider these extensions, but note that if the multidimensional renewal model is appropriately formulated, our margins should remain valid since they only require linear control systems theory to hold.

We take Laplace transforms of Eq. (10) to construct Eq. (11), which is amenable to our gain and delay margin controllability analyses. We sketch the architecture of this model in Fig. 4(b),

$$L(s) = -\sum_{n=1}^{N} \epsilon_n R_n W_n(s) K_n(s), \quad G(s) = \frac{1}{1 + L(s)}. \quad (11)$$

Using the fact that $W_n(0) = 1$, we find that if $\omega_{PC} = 0$ then $M_G = |-\sum_{n=1}^{N} K_n(0)\epsilon_n R_n|^{-1}$. We can therefore scale the epidemic by a quantity that is a weighted sum of control, reproduction numbers, and proportions of the contributing infectious types. As we showed in the above sections, this condition is only likely to be met if every controller is constant (at which also $M_D \to \infty$). If controllers introduce dynamics, which is realistic, then we expect effects similar to Fig. 3.

Equation (11) provides the flexibility to investigate several controllability problems. We focus on two questions about the limitations of targeted control for heterogeneous populations. We let $N = 2$ and assume that $R_1 \geq R_2$ so that type 1 represents individuals with the more transmissible variant or superspreading nodes. We consider nonselective control where $K_1(s) = K_2(s) = K(s)$ and targeted control, in which only one type is controlled. We target only type 1, which is more transmissible, so type 2 is uncontrolled and $K_2(s) = 1$. Our first question asks under what conditions the targeted approach, which is often proposed as an efficient control scheme [11,41], fails to suppress the overall epidemic, making nonselective control unavoidable. For this two-type epidemic $L(s) = -[\epsilon_1 R_1 K_1(s) W_1(s) + \epsilon_2 R_2 W_2(s)]$ for targeted control and $-K(s)[\epsilon_1 R_1 W_1(s) + \epsilon_2 R_2 W_2(s)]$ for nonselective control, with $\epsilon_2 = 1 - \epsilon_1$.
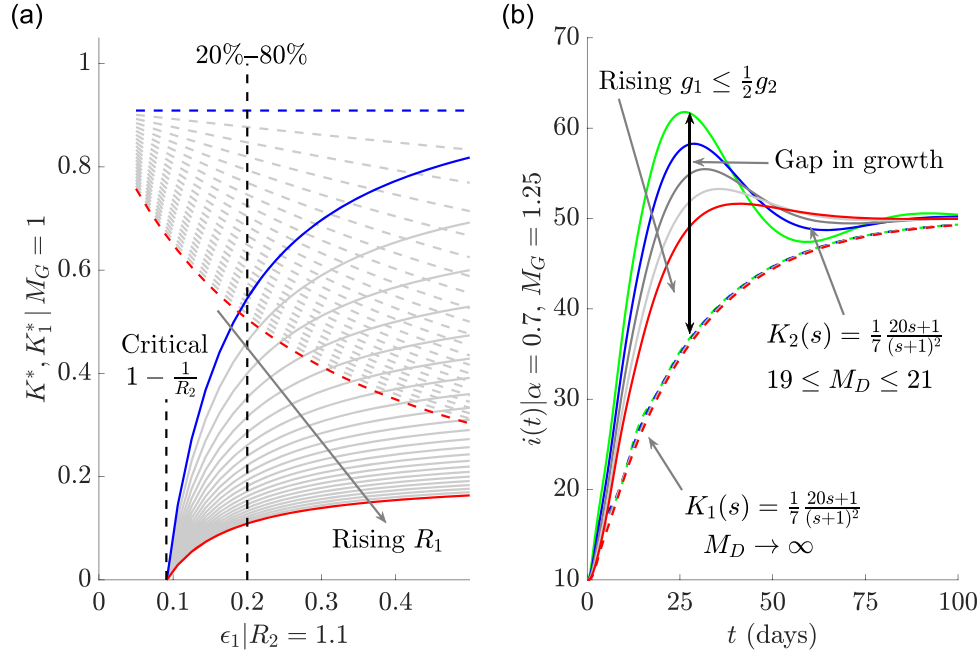
FIG. 6.   Targeted control in multitype epidemics. We explore controllability and performance limits for epidemics that involve two distinct types, modeling superspreading or cocirculating variants. Panel (a) plots the constant control effort necessary for critical stability ($M_G = 1$) under a nonselective strategy with controller K^* that reduces infections of both types (dashed) and a targeted strategy with controller K_1^* that reduces only infections of type 1 (solid), which has larger transmissibility $R_1 \geq R_2 = 1.1$. For both strategies, we vary the proportion of type 1, ϵ_1, and curves are for increasing R_1 from blue (1.1) to red (5.5) with intermediate values in gray. We use a vertical line to show the ϵ_1 for the commonly used 20–80 superspreading rule that describes realistic epidemic heterogeneity. Targeted control requires substantially more effort (as it must also account for the uncontrolled type 2), and the epidemic is uncontrollable if ϵ_1 is smaller than the critical vertical line [see Eq. (12)]. Panel (b) considers targeted controllers that introduce dynamics and apply only $K_1(s)$ or $K_2(s)$ to reduce either type-1 or -2 infections. We fix $\epsilon_1 R_1 = \epsilon_2 R_2 = \alpha$ so that all types contribute to overall transmissibility equally and both controllers lead to the same $M_G > 1$. We illustrate how new infections $i(t)$ change due to both schemes (dashed and solid, respectively), where type 1 is the faster variant possessing mean generation time $g_1 \leq g_2 = 8$ days. Targeting the slower type 2 leads to worse performance (including faster transient growth) and is sensitive to g_1 (curves are not grouped).

In both cases, $\omega_{PC} = 0$ and $W_1(0) = W_2(0) = 1$ (see Sec. II). If we apply only constant controllers, then $M_D \to \infty$, and controllability is exclusively defined by the values of M_G, which are computed as $|\epsilon_1 R_1 K_1(0) + \epsilon_2 R_2|^{-1}$ and $|K(0)|^{-1}|\epsilon_1 R_1 + \epsilon_2 R_2|^{-1}$. To attain some specific M_G, we require $K_1(0) = (M_G^{-1} - \epsilon_2 R_2)(\epsilon_1 R_1)^{-1}$ and $K(0) = M_G^{-1}(\epsilon_1 R_1 + \epsilon_2 R_2)^{-1}$. We can combine these relations to get the left side of Eq. (12), which shows how much smaller $K_1(0)$ needs to be than $K(0)$, i.e., how much more targeted control effort is required to attain our desired M_G,

$$K_1(0) = K(0) - \left(\frac{\epsilon_2 R_2}{\epsilon_1 R_1}\right)(1 - K(0)), \quad \epsilon_1 \geq 1 - \frac{1}{M_G R_2}.$$
(12)

We plot the control efforts $K^* = K(0)$ and $K_1^* = K_1(0)$ from both strategies that are necessary to achieve critical stability ($M_G = 1$) in Fig. 6(a). There we observe the limits of targeted control as a critical ϵ_1 cutoff (dashed vertical). This follows from the positivity constraint $0 \leq K_1(0) < 1$, where 1 is no control and 0 defines perfect control, in which

type-2 infections are neutralized. We derive this for any desired gain margin on the right side of Eq. (12). Interestingly, this cutoff does not depend on R_1 and, if $M_G = 1$, it indicates that targeted control works only when the proportion of superspreading nodes or type-1 variants is above $1 - R_2^{-1}$. This procedure is easily generalized to N-type epidemics where we can control a subset χ of the types. The controllability cutoff then requires the uncontrolled proportion $|\sum_{n \notin \chi} \epsilon_n R_n W_n(s)| \leq M_G^{-1}$.

Our second question relates to the interaction between differing generation times of the types and induced controller dynamics. We consider targeted control of either type or variant with type 1 having smaller mean generation time and hence being faster than type 2, i.e., $g_1 \leq g_2$. We set $\epsilon_1 R_1 = \epsilon_2 R_2 = \alpha$ to remove any relative transmissibility advantage between the types. Consequently, variations in the infections caused by the types emerge from their generation time distribution differences. Targeted control applies nonconstant control $K_1(s)$ exclusively to type 1 or $K_2(s)$ exclusively to type 2, yielding loop TFs $L(s) = -\alpha[K_1(s)W_1(s) + W_2(s)]$ and $-\alpha[W_1(s) + K_2(s)W_2(s)]$.

Because the controller induces additional dynamics, we are neither guaranteed $\omega_{\mathrm{PC}} = 0$ nor $M_D \to \infty$ and must evaluate the complete (M_D, M_G) pair.

We compute these margins and dynamical responses to constant importations in Fig. 6(b) for a range of fast type-1 generation time distributions $w_1(t)$ and a fixed (slow) type-2 distribution $w_2(t)$. Although M_G is the same for both schemes, controlling type 2, which may occur when transmission chains of slower variants are easier to interrupt, yields worse performance. The overshoots and oscillations are also accompanied by a finite M_D, highlighting that neglecting the faster variant can potentially reduce robustness of the controlled epidemic to perturbations or equally reduce controllability below what we may expect from conventional measures based on reproduction numbers or asymptotic growth rates. For certain controllers (not shown), we also find that $\omega_{\mathrm{PC}} > 0$ can occur and reduce M_G for either targeted scheme. This underscores the importance of our two-margin solution to understanding controllability.

IV. DISCUSSION

Measuring the controllability of an infectious disease subject to various intervention options is a fundamental contribution of mathematical modeling to epidemiology [4,12]. However, there exists no rigorous and precise definition of what controllability means [8,10] and studies have highlighted a need for robust analytical frameworks to better appraise the impacts of targeted and reactive interventions [1]. Currently, the distance from the epidemic threshold of $R = 1$ or $r = 0$ is frequently used to measure controllability. Here we demonstrated that this notion of controllability, although reasonable, is idealistic and likely misleading because neither R nor r completely and unambiguously measures distance from stability. We proposed an alternative and analytic definition of this distance by reformulating the disease transmission process as a positive feedback loop and leveraging results from control engineering [31].

We derived epidemic transfer functions to describe the dynamics of this loop and model how stabilizing interventions interrupt and attenuate this positive feedback (e.g., by blocking new infections through quarantines). For already stable or controlled epidemics, we tested robustness to perturbations or uncertainties that amplify infections along this loop (e.g., by relaxing any interventions or from pathogenic variants). This allowed us to develop stability margins that accurately measure the distance from stability (Fig. 1) in units of the scale and speed of the required control efforts. The gain and delay margins are key metrics from control engineering [17,18], a field that studies stability and feedback problems across many dynamical systems. Although there is increasing interest in using tools from this field to better understand infectious disease spread [9,46–49],

our study appears to be among the earliest to construct margins for epidemics and appraise existing notions of disease controllability.

Our central contribution is a flexible method for quantifying epidemic controllability that is both computable and easily interpreted across many salient characteristics of infectious diseases. This is important for three main reasons. First, R and r can lose their meaning or comparability as threshold parameters when characteristics such as superspreading and multitype spread are included [24,50]. Second, for a given transmission model there can be numerous ways of constructing and defining valid epidemic thresholds, and these are not always consistent when assessing interventions [25,45,50]. For example, when interventions change generation times, then we can find situations where r increases yet R decreases [51]. Third, earlier frameworks were unable to directly include reactive or feedback effects within their measures and did not account for how the implementation of interventions might modify effectiveness.

In contrast, our gain and delay margins maintain their interpretation, validity, uniqueness, and comparability across complex disease models and explicitly reflect feedback loops intrinsic to transmission and intervention. These properties allowed controllability to be measured across realistic generation time distributions (Fig. 2), constraints on interventions (Fig. 3), surveillance imperfections (Fig. 5), and transmission heterogeneities (Fig. 6). Principal insights emerging from this unified approach were that (i) R and r only track controllability in restrictive settings where interventions do not alter temporal disease characteristics and are applied instantly, (ii) sharp thresholds of controllability exist due to presymptomatic spread, superspreading, delays, and underreporting and cocirculating variants that generalize $1 - 1/R$-type results, and (iii) the delay margin is crucial because lags along feedback loops (from both intervention delays and surveillance biases) can destabilize epidemics that are conventionally deemed controlled.

While our approach rigorously incorporates many realistic epidemic complexities and extends earlier frameworks [1,8,10], it depends on several simplifying assumptions, which we made to ensure tractability and to extract general insights. Specifically, our analysis uses deterministic renewal models and assumes constant R or r. Although some or all of these assumptions are common to seminal studies and recent works on controllability thresholds [1,43], the influence of stochasticity in disease transmission can be substantial [7,11]. We recommend computing our margins to initially assess intervention impact and then using them to guide the running of more complex stochastic models. Our margins are only well defined for linear systems, which include epidemics describable by renewal models with constant R. If R varies on the timescale of interventions or involves nonlinear effects such as

saturation or susceptible depletion, this assumption may be invalidated. However, we can use piecewise-constant transmissibility approximations and fit renewal models to each piece, to partially circumvent this issue.

Moreover, we examined linear and reactive control actions only (i.e., convolutions of kernels with past infections). This improves upon many studies, where controllers simply multiply and reduce R or r but may not model other notable types of interventions, such as those reducing infections due to nonlinear switching triggers or those that completely ignore feedback signals in favor of predetermined action [34,53]. Understanding the relative benefits of these different strategies is an ongoing area of research. Last, we comment that controllability here focused on intrinsic epidemic dynamics and neglected the costs of actions. Including how these costs further constrain the realizable limits of controllability, as well as incorporating key behavioral effects within our feedback loops are the future directions of this research.

In summary, we demonstrated that controllability is completely and accurately measured only by the distance of the loop transfer function $L(s)$ from -1. This generalizes and improves upon the conventionally used distances of R from 1 or r from 0, but still admits interpretable margins or safety factors that quantify how much we can scale infections or delay interventions to attain critical stability. This allows us to better evaluate when targeted interventions are insufficient and hence when nonselective controls such as lockdowns are justified from the viewpoint of curbing transmission. We found that targeted controls fail when the dynamics of the unobserved or untargeted infectious population, together with constraints on surveillance and intervention implementation, cross margin thresholds that are analytically derived from our framework.

All data and code underlying the analyses and figures within this study are freely available in MATLAB on GitHub [33].

ACKNOWLEDGMENTS

[1] C. Fraser, S. Riley, R. M. Anderson, and N. M. Ferguson, *Factors that make an infectious disease outbreak controllable*, Proc. Natl. Acad. Sci. U.S.A. **101**, 6146 (2004).

[2] K. T. D. Eames and M. J. Keeling, *Contact tracing, and disease control*, Proc. Biol. Sci. **270**, 2565 (2003).

[3] N. Ferguson, D. Laydon, G. Nedjati-Gilani *et al.*, Report 9: Impact of non-pharmaceutical interventions (NPIs) to reduce COVID-19 mortality and healthcare demand, 10.25561/77482, 2020.

[4] H. W. Hethcote, *The mathematics of infectious diseases*, SIAM Rev. **42**, 599 (2000).

[5] WER Team, *Ebola virus disease in West Africa—The first 9 months of the epidemic and forward projections*, N. Engl. J. Med. **371**, 1481 (2014).

[6] M. J. Walport, *Professor Sir Mark Walport on behalf of the Expert Working Group for the Royal Society's programme on non-pharmaceutical interventions. Executive summary to the Royal Society report "COVID-19: Examining the effectiveness of non-pharmaceutical interventions,"* Phil. Trans. R. Soc. A **381**, 20230211 (2023).

[7] C. T. Bauch, J. O. Lloyd-Smith, M. P. Coffee, and A. P. Galvani, *Dynamically modeling SARS and other newly emerging respiratory illnesses: Past, present, and future*, Epidemiology **16**, 791 (2005).

[8] C. M. Peak, L. M. Childs, Y. H. Grad, and C. O. Buckee, *Comparing nonpharmaceutical interventions for containing emerging epidemics*, Proc. Natl. Acad. Sci. U.S.A. **114**, 4023 (2017).

[9] F. Casella, *Can the COVID-19 epidemic be controlled on the basis of daily test reports?* IEEE Control Syst. Lett. **5**, 1079 (2021).

[10] J. M. McCaw, K. Glass, G. N. Mercer, and J. McVernon, *Pandemic controllability: A concept to guide a proportionate and flexible operational response to future influenza pandemics*, J. Public Health **36**, 5 (2014).

[11] J. O. Lloyd-Smith, S. J. Schreiber, P. E. Kopp, and W. M. Getz, *Superspreading and the effect of individual variation on disease emergence*, Nature (London) **438**, 355 (2005).

[12] R. Anderson, C. Donnelly, D. Hollingsworth, M. Keeling, C. Vegvari, and R. Baggaley, *Reproduction number (R) and growth rate (r) of the COVID-19 epidemic in the UK: Methods of, The Royal Society* (2020), https://royalsociety.org/-/media/policy/projects/set-c/set-covid-19-r-estimates.pdf.

[13] L. Ferretti, C. Wymant, M. Kendall, L. Zhao, A. Nurtay, L. Abeler-Dörner, M. Parker, D. Bonsall, and C. Fraser, *Quantifying SARS-CoV-2 transmission suggests epidemic control with digital contact tracing*, Science **368**, eabb6936 (2020).

[14] K. H. Grantz, E. C. Lee, L. D'Agostino McGowan, K. H. Lee, C. J. E. Metcalf, E. S. Gurley, and J. Lessler, *Maximizing and evaluating the impact of test-trace-isolate programs: A modeling study*, PLoS Med. **18**, e1003585 (2021).

[15] J. Wallinga and M. Lipsitch, *How generation intervals shape the relationship between growth rates and reproductive numbers*, Proc. R. Soc. B **274,** 599 (2007).

[16] R. Pates, A. Ferragut, E. Pivo, P. You, F. Paganini, and E. Mallada, *Respect the unstable: Delays and saturation in contact tracing for disease control*, SIAM J. Control Optim. **60,** S196 (2022).

[17] K. Ogata, *Modern Control Engineering* (Prentice-Hall, Englewood Cliffs, NJ, 1997), Vol. 1.3.

[18] K. J. Åström and R. M. Murray, *Feedback Systems: An Introduction for Scientists and Engineers* (Princeton University Press, Princeton, NJ, 2010).

[19] T. Churcher, J. Cohen, S. Ntshalintshali, S. Kunene, and S. Cauchemez, *Measuring the path toward malaria elimination*, Science **344,** 1230 (2014).

[20] K. Sun, W. Wang, L. Gao, Y. Wang, K. Luo, L. Ren *et al.*, *Transmission heterogeneities, kinetics, and controllability of SARS-CoV-2*, Science **371,** eabe2424 (2021).

[21] S. T. Ali, L. Wang, E. H. Y. Lau, X.-K. Xu, Z. Du, Y. Wu, G. M. Leung, and B. J. Cowling, *Serial interval of SARS-CoV-2 was shortened over time by nonpharmaceutical interventions*, Science **369,** 1106 (2020).

[22] M. Favero, G. Scalia Tomba, and T. Britton, *Modelling preventive measures and their effect on generation times in emerging epidemics*, J. R. Soc. Interface **19,** 20220128 (2022).

[23] I. Stott, D. J. Hodgson, and S. Townley, *Beyond sensitivity: Nonlinear perturbation analysis of transient dynamics*, Methods Ecol. Evol. **3,** 673 (2012).

[24] L. Pellis, F. Ball, and P. Trapman, *Reproduction numbers for epidemic models with households and other social structures, I. Definition and calculation of R0*, Math. Biosci. **235,** 85 (2012).

[25] K. V. Parag and U. Obolski, *Risk averse reproduction numbers improve resurgence detection*, PLoS Comput. Biol. **19,** e1011332 (2023).

[26] C. Fraser, *Estimating individual and household reproduction numbers in an emerging epidemic*, PLoS One **2,** e758 (2007).

[27] A. Cori, N. M. Ferguson, C. Fraser, and S. Cauchemez, *A new framework and software to estimate time-varying reproduction numbers during epidemics*, American Journal of Epidemiology **178,** 1505 (2013).

[28] M. G. Roberts and H. Nishiura, *Early estimation of the reproduction number in the presence of imported cases: Pandemic influenza H1N1-2009 in New Zealand*, PLoS One **6,** e17835 (2011).

[29] D. R. Cox, *A use of complex probabilities in the theory of stochastic processes*, Math. Proc. Cambridge Philos. Soc. **51,** 313 (1955).

[30] H. Lee and H. Nishiura, *Sexual transmission and the probability of an end of the Ebola virus disease epidemic*, J. Theor. Biol. **471,** 1 (2019).

[31] S. Skogestad and I. Postlethwaite, *Multivariable Feedback Control: Analysis and Design*, 2nd ed. (John Wiley & Sons, New York, 2005).

[32] P. Seiler, A. Packard, and P. Gahinet, *An introduction to disk margins (lecture notes)*, IEEE Control Syst. Mag. **40,** 78 (2020).

[33] Kris Parag, *EpidemicControllability, v1.0* (2023), https://github.com/kpzoo/EpidemicControllability/releases/tag/v1.0.

[34] J. Hu, G. Qi, X. Yu, and L. Xu, *Modeling, and staged assessments of the controllability of spread for repeated outbreaks of COVID-19*, Nonlinear Dyn. **106,** 1411 (2021).

[35] D. H. Morris, F. W. Rossine, J. B. Plotkin, and S. A. Levin, *Optimal, near-optimal, and robust epidemic control*, Commun. Phys. **4,** 78 (2021).

[36] S. Cauchemez, P. Bosetti, and B. J. Cowling, *Managing sources of error during pandemics*, Science **379,** 437 (2023).

[37] P. Yan and G. Chowell, *Quantitative Methods for Investigating Infectious Disease Outbreaks* (Springer, Cham, 2019).

[38] K. V. Parag, C. A. Donnelly, and A. E. Zarebski, *Quantifying the information in noisy epidemic curves*, Nat. Comput. Sci. **2,** 584 (2022).

[39] E. Goldstein, J. Dushoff, J. Ma, J. B. Plotkin, D. J. D. Earn, and M. Lipsitch, *Reconstructing influenza incidence by deconvolution of daily mortality time series*, Proc. Natl. Acad. Sci. U.S.A. **106,** 21825 (2009).

[40] G. Pullano, L. Di Domenico, C. E. Sabbatini, E. Valdano, C. Turbelin, M. Debin *et al.*, *Underdetection of cases of COVID-19 in France threatens epidemic control*, Nature (London) **590,** 134 (2021).

[41] N. J. Irons and A. E. Raftery, *Estimating SARS-CoV-2 infections from deaths, confirmed cases, tests, and random surveys*, Proc. Natl. Acad. Sci. U.S.A. **118,** e2103272118 (2021).

[42] M. Woolhouse, C. Dye, J. Etard *et al.*, *Heterogeneities in the transmission of infectious agents: Implications for the design of control programs*, Proc. Natl. Acad. Sci. U.S.A. **94,** 338 (1997).

[43] F. Blanquart, N. Hozé, B. J. Cowling, F. Débarre, and S. Cauchemez, *Selection for infectivity profiles in slow and fast epidemics, and the rise of SARS-CoV-2 variants*, eLife **11,** e75791 (2022).

[44] T. Britton, F. Ball, and P. Trapman, *A mathematical model reveals the influence of population heterogeneity on herd immunity to SARS-CoV-2*, Science **369,** 846 (2020).

[45] K. Glass, G. N. Mercer, H. Nishiura, E. S. McBryde, and N. G. Becker, *Estimating reproduction numbers for adults and children from case data*, J. R. Soc. Interface **8,** 1248 (2011).

[46] J. M. Heffernan, R. J. Smith, and L. M. Wahl, *Perspectives on the basic reproductive ratio*, J. R. Soc. Interface **2,** 281 (2005).

[47] C. Nowzari, V. M. Preciado, and G. J. Pappas, *Analysis and control of epidemics: A survey of spreading processes on complex networks*, IEEE Control Syst. Mag. **36,** 26 (2016).

[48] G. Stewart, K. van Heusden, and G. A. Dumont, *How control theory can help us control COVID-19*, https://spectrum.ieee.org/how-control-theory-can-help-control-covid19.

[49] K. V. Parag, B. J. Cowling, and C. A. Donnelly, *Deciphering early-warning signals of SARS-CoV-2 elimination and resurgence from limited data at multiple scales*, J. R. Soc. Interface **18,** 20210569 (2021).

[50] G. Giordano, F. Blanchini, R. Bruno, P. Colaneri, A. Di Filippo, A. Di Matteo, and M. Colaneri, *Modelling the COVID-19 epidemic and implementation of population-wide interventions in Italy*, Nat. Med. **26**, 855 (2020).

[51] J. Li, D. Blakeley, and R. J. Smith, *The failure of R0*, Comput. Math. Methods Med. **2011**, 527610 (2011).

[52] K. V. Parag, B. J. Cowling, and B. C. Lambert, *Angular reproduction numbers improve estimates of transmissibility when disease generation times are misspecified or time-varying*, Proc. Biol. Sci. **290**, 20231664 (2023).

[53] M. Bin, P. Y. K. Cheung, E. Crisostomi, P. Ferraro, H. Lhachemi, R. Murray-Smith *et al.*, *Post-lockdown abatement of COVID-19 by fast periodic switching*, PLoS Comput. Biol. **17**, e1008604 (2021).